Impact of Power Grid Strength and PLL Parameters on Stability of Grid-Connected DFIG Wind Farm

Ju Liu, Wei Yao, *Senior Member, IEEE*, Jinyu Wen, *Member, IEEE*, Jiakun Fang, *Member, IEEE*, Lin Jiang, *Member, IEEE*, Haibo He, *Fellow, IEEE*, and Shijie Cheng, *Life Fellow, IEEE*

***Abstract*—This paper investigates the impact of power grid strength and phase-locked loop (PLL) parameters on small signal stability of grid-connected doubly-fed induction generator (DFIG)-based wind farm. Modal analysis of the grid-connected DFIG wind turbine under different operating conditions and various power grid strengths are investigated at first. Modal analysis results reveal that the DFIG connected to a weak grid may easily lose stability under the heavy-duty operating conditions due to PLL oscillation. The object of this paper is to identify the PLL oscillation mechanism as well as influence factors and propose a damping solution for this oscillation mode. A simplified linear system model of the grid-connected DFIG wind turbine is proposed for analyzing the PLL oscillation. Through the complex torque coefficients method and using this model, the oscillation mechanism and influence factors including the power grid strength and the PLL parameters are identified. To suppress this PLL oscillation, a mixed H_2/H_∞ robust damping controller is proposed and designed for the DFIG. Electromagnetic transient simulation results of both single-DFIG system and multiply-DFIG system verify the correctness of the analysis results and effectiveness of the proposed damping controller.**

***Index Terms*—Doubly-fed induction generator (DFIG), small signal stability, phase-locked loop (PLL), power grid strength, damping controller.**

NOMENCLATURE

β	Pitch angle
λ	Tip speed ratio
ω_B	Base speed at the rated frequency
ω_r	Speeds of wind generator
ω_t	Speeds of wind turbine
ρ	Air density
θ_s	Torsion angle of shaft
B_s	Damping coefficient
c, g	GSC and grid components
$C_p(\beta,\lambda)$	Wind turbine power coefficient
dq	Direct- and quadrature-axis components in rotating dq reference frame
$E_d^{'}, E_q^{'}$	Equivalent internal dq-axis voltages
H_g	Inertia constant of wind generator
H_t	Inertia constant of wind turbine
i	Current
i_{sd}, i_{sq}	Stator dq-axis currents
K	Gain coefficient
K_s	Stiffness coefficient
L_m, L_{rr}, L_{ss}	Stator, rotor, and mutual inductances
p	Signals measured in PLL reference frame
P, I	Proportional and integral components
p, i	Power and current control loop components
P, Q	Active and reactive power
P_m	Mechanical power of wind turbine
R	Rotor radius
$R_s, X_s, X_s^{'}$	Stator resistance, reactance and transient reactance
s, r	Stator and rotor components
S_{tip}	Short-circuit ratio at the PCC bus
S_{wf}	Rated power of wind farm
$T_0^{'}$	Stator transient open circuit time constant
T_e	Electromagnetic torque
T_m	Mechanical torque
U	Voltage
U_{rd}, U_{rq}	Rotor dq-axis voltages
U_{sd}, U_{sq}	Stator dq-axis voltages
v_w	Wind speed
Z_{wf}	Equivalent impedance of the wind power transmission system
*	Values of reference

Manuscript received May 30, 2018; revised October 2, 2018, December 18, 2018; accepted February 2, 2019. This work was supported by National Natural Science Foundation of China under Grant 51577075. Paper no. TSTE-00510-2018 *(Corresponding author: Wei Yao.)*

J. Liu, W. Yao, J. Y. Wen, and S. J. Cheng are with State Key Lab of advanced Electromagnetic Engineering and Technology, School of Electrical and Electronic Engineering, Huazhong University of Science and Technology, Wuhan, 430074. P. R. China. Currently, Dr J. Liu is also working at the State Grid Hubei economic and Research Institute, Wuhan, 430000. P. R. China. (E-mail: w.yao@hust.edu.cn).

J. K. Fang is with Department of Energy Technology, Aalborg University, Aalborg, DK9220, Denmark.

L. Jiang is with Department of Electrical Engineering and Electronics, The University of Liverpool, Liverpool, L69 3GJ, U. K.

H. B. He is with the Department of Electrical, Computer and Biomedical Engineering, University of Rhode Island, Kingston, RI 02881, USA.

I. INTRODUCTION

THE increasing integration of wind power into the power system will weaken the power grid strength, and the short-circuit ratio (SCR) at the point of common coupling (PCC) of wind farm integration will become lower [1]–[3]. Hence, the wind farm is more sensitive to disturbances, which would deteriorate the stability of the wind power system [4]–[7]. Especially in the regions where wind energy is far away from the main power grid, like Northwest China, bulk wind energy is traveled thousands of kilometers to load centers via long transmission lines [8]. In recent years, several power oscillation accidents have occurred, which led to wind turbines tripping and caused the instability of power systems [9], [10].

Unlike the low frequency oscillation with frequency ranging from 0.2Hz to 2.5Hz, the frequency of the wind power system

oscillation ranges from several to dozens of Hz [11], which is within the frequency range of sub-synchronous oscillation. Thus, references [11]–[13] formed a set of methods based on frequency scan and the complex-damping-coefficient analysis to reveal the mechanism of these oscillations. Moreover, different control strategies are proposed to suppress such oscillations. However, the aforementioned investigations mainly focus on the power oscillations occurring in the system that wind power is delivered through series compensated or high voltage direct current (HVDC) transmission lines [14]. They are not applicable to the conditions, in which wind power is exported via alternating current transmission lines without series compensation.

On the other hand, when wind power is delivered by a long-distance AC transmission line, the electrical connection between the wind farm and external power grid is weak. The power grid strength, which is used to describe the strength of the electrical connection between the wind farm and external power grid and parameterized by SCR at the PCC bus of the wind farm, may be very low. In some cases, the SCR at the PCC bus of the wind farm is even lower than 3, which satisfies the weak grid condition defined by the IEEE Transmission and Distribution Committee as SCR$<$3 [15]. Therefore, there would be stability problems of the PLL-based voltage source converter (VSC) [16]–[19] connected to a weak grid. It has been found that the PLL plays an important role in the stability of grid-connected VSC, for example, the VSC-HVDC converter connected to a weak power grid [16]–[18] and Type 4 wind turbine (PMSG) connected to a weak grid [20], [21]. However, very few references take the PLL block as a main issue into consideration when the stability of the grid-connected DFIG wind farm is analyzed [22]. The power oscillation problem has threatened the stability of the wind integrated power system as the penetration level increases. And for the grid-connected DFIG based wind turbines, the power oscillations could be observed at the transmission line of wind integrated power system. Consequently, it is necessary to establish a detailed model of grid-connected DFIG wind turbines including the PLL block to analyze the oscillatory interactions between the wind farm and the grid. What is more, the influence of the power grid strength and the PLL parameters on the stability of grid-connected DFIG based wind farm also need to be investigated in detail.

In [23], [24], it is suggested that the impact of the PLL must be considered when the DFIG based wind farm integrates into a weak grid. During the process of the low voltage ride through of the wind farm, the coupling between the wind farm and the external AC power grid is weak because the voltage at the PCC bus is relatively low. When the dynamic characteristic of the PLL is considered, the loss of synchronism [25] and DC voltage oscillation [26], [27] will occur in some situations. Also, when the wind farm is connected into a weak grid under normal condition, it is reported in [28] that, when the PLL mode is poorly damped and its frequency falls into the frequency range of electromechanical oscillations, it would greatly participate in electromechanical modes. However, the cause of the controller-interfaced oscillation involving the PLL is not explained. By using the eigenvalue analysis, it can be found that the dynamic of the PLL oscillation mode will occur under serious condition if the line parameter is large enough [29], [30]. However, the oscillation mechanism of the PLL mode and how to improve the damping ratio of the PLL mode still need to be further investigated.

To fill this gap, this paper conducts modal analysis to show that the PLL oscillation mode is the main reason leading to instability of the grid-connected DFIG wind turbine. The object of this paper is to identify the PLL oscillation mechanism as well as influence factors and propose a damping solution for this oscillation mode. The impacts of the PLL parameters and the power grid strengths on the PLL oscillation mode are analyzed by using complex torque method and the proposed simplified linear model. In addition, a mixed H_2/H_∞ robust damping controller is proposed to suppress the PLL oscillation phenomenon. Electromagnetic transient simulations are conducted to verify the correctness of the analysis results and effectiveness of the proposed damping controller.

In conclusion, the main contributions of this paper are:

- Modal analysis results reveal that the DFIG connected to a weak grid may easily lose stability under the heavy-duty operating conditions due to PLL oscillation.
- A simplified linear system model of the grid-connected DFIG wind turbine is proposed. Through the complex torque coefficients method and using this model, the oscillation mechanism and influence factors including the power grid strength and the PLL parameters are identified.
- To suppress this PLL oscillation, a mixed H_2/H_∞ robust damping controller is proposed and designed for the DFIG. Simulation validation is also conducted.

The rest of this paper is organized as follows. Section II gives the model of the grid-connected DFIG wind farm. In Section III, the modal analysis of the grid-connected DFIG wind farm are analyzed. The simplified model of the grid-connected DFIG wind farm is proposed and instability mechanism is investigated in Section IV. In Section V, a mixed H_2/H_∞ robust damping controller is proposed to suppress the PLL oscillation. Case studies are undertaken in Section VI. Conclusions are drawn in Section VII.

II. Model of Grid-Connected DFIG Wind Turbine

The dynamic model of the grid-connected DFIG wind turbine is recalled in this section including the mechanical part, generator part, rotor side converter, and PLL.

A. Model of the Mechanical Part

The mechanical part of the wind turbine is mainly to capture wind energy and convert it into kinetic energy. According to the theory of aerodynamics, the captured wind power P_m at wind speed v_w is:

$$P_m = \frac{1}{2} C_p(\beta, \lambda) \rho \pi R^2 v_w^3 \tag{1}$$

The wind turbine, generator, gearbox, and shafts could be modeled as a two-mass drive train. The low-speed shaft and wind turbine equal to one mass, while the other mass

represents the high-speed shaft and wind generator. The mathematical description of such two-mass driven system is [32]:

$$\begin{cases} 2H_t\dfrac{d\omega_t}{dt} = T_m - K_s\theta_s - B_s\dfrac{d\theta_s}{dt} \\ 2H_g\dfrac{d\omega_r}{dt} = K_s\theta_s + B_s\dfrac{d\theta_s}{dt} - T_e \\ \dfrac{d\theta_s}{dt} = \omega_B(\omega_t - \omega_r) \end{cases} \tag{2}$$

B. Model of the Generator

Under balanced and unsaturated conditions, in the dq-frame, the stator voltage equation of DFIG is given as follow [32]:

$$\begin{cases} \dfrac{X_s'}{\omega_B}\dfrac{d}{dt}i_{sd} = -(R_s + \dfrac{X_s - X_s'}{T_0'})i_{sd} - X_s'i_{sq} + \omega_r E_d' + \dfrac{1}{T_0'}E_q' - U_{sd} + \dfrac{L_m}{L_{rr}}U_{rd} \\ \dfrac{X_s'}{\omega_B}\dfrac{d}{dt}i_{sq} = -(R_s + \dfrac{X_s - X_s'}{T_0'})i_{sq} + X_s'i_{sd} + \omega_r E_q' - \dfrac{1}{T_0'}E_d' - U_{sq} + \dfrac{L_m}{L_{rr}}U_{rq} \\ \dfrac{1}{\omega_B}\dfrac{d}{dt}E_d' = -\dfrac{X_s - X_s'}{T_0'}i_{sq} - (1-\omega_r)E_q' - \dfrac{1}{T_0'}E_d' + \dfrac{L_m}{L_{rr}}U_{rq} \\ \dfrac{1}{\omega_B}\dfrac{d}{dt}E_q' = \dfrac{X_s - X_s'}{T_0'}i_{sd} + (1-\omega_r)E_d' - \dfrac{1}{T_0'}E_q' - \dfrac{L_m}{L_{rr}}U_{rd} \end{cases} \tag{3}$$

C. Model of the Rotor Side Converter

The control of the rotor side converter plays an important role in the operation characteristics of DFIG wind turbines. The main goal of the rotor side converter is to realize the maximum power point tracking (MPPT) control of active power and the unity power factor control of reactive power. When U_{rid} and U_{riq} are taken as the disturbance terms to conduct feed-forward compensation, the current inner-loop vector control equation of the rotor side converter can be represented as follows [32]:

$$\begin{cases} U_{rd}^* = -(K_{riP} + \dfrac{K_{riI}}{s})(i_{rd}^* - i_{rd}) + U_{rid} \\ U_{rq}^* = -(K_{riP} + \dfrac{K_{riI}}{s})(i_{rq}^* - i_{rq}) + U_{riq} \end{cases} \tag{4}$$

Ignoring the impact of the stator flux and the terminal voltage, the active power output of the wind turbine mainly depends on the d-axis rotor current, the reactive power output mainly depends on the q-axis rotor current, so the control strategy of the power outer-loop is [12]:

$$\begin{cases} i_{rd}^* = -(K_{rpP} + \dfrac{K_{rpI}}{s})(P_s^* - P_s) \\ i_{rq}^* = -(K_{rpP} + \dfrac{K_{rpI}}{s})(Q_s^* - Q_s) \end{cases} \tag{5}$$

D. Model of the PLL

The proportional and integral (PI)-based PLL in the generic synchronous frame is shown in Fig. 1, where K_P and K_I are the proportional and integral coefficients of the PLL. The input voltage $U\angle\alpha$ satisfies:

$$U_q^p = U\sin(\theta^p - \alpha) \approx U(\theta^p - \alpha) \tag{6}$$

The linearization model of the PLL system can be represented as:

$$\begin{cases} s\Delta\theta^p(s) = \Delta\omega^p(s) \\ \Delta\omega^p(s) = -\Delta U_q^p(s)(K_P + K_I/s) \end{cases} \tag{7}$$

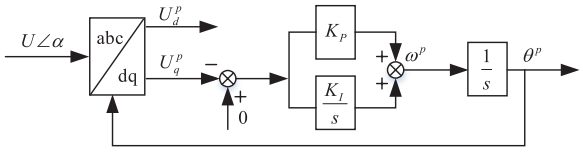

Fig. 1. PLL structure based on d-axis orientation

If $U_q^p = 0$, the phase angle θ^p obtained by the PLL is the same with the phase angle α of the input voltage, which realizes the phase tracking. However, when the external power system is weak, oscillation will occur at the PLL loop. The frequency calculated by the differential of θ^p oscillates and deviates from 50 Hz. By affecting rotor side converter control signals, this oscillation would lead to the oscillation of the DFIG output power. The dynamic characteristic of the PLL is usually neglected for small signal stability analysis of DFIG [18], [19]. In this paper, to take the influence of the PLL into account, the dq voltages U_{rdq}' and currents I_{rdq}' of the rotor side converter should be obtained by using the phase θ^p observed by the PLL.

E. Single Grid-Connected DFIG Wind farm

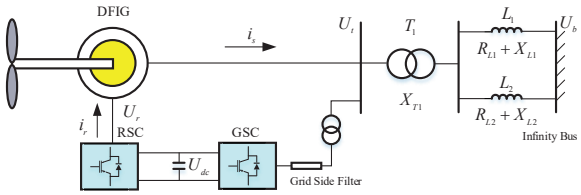

Fig. 2. Single grid-connected DFIG wind farm

For a single grid-connected DFIG wind farm illustrated in Fig. 2, this paper defines the SCR at the PCC bus of the wind farm, named S_{tip}, as the ratio of the short-circuit capacity to the rated capacity of the wind farm. Thus, the SCR at the PCC bus equals to the ratio of the equivalent admittance of the wind power transmission system to the rated power of the wind farm:

$$S_{tip} = 1/(|Z_{wf}|S_{wf}) \tag{8}$$

F. Flowchart of the Proposed Approach

After building the detailed model of the grid-connected DFIG wind farm, an approach is proposed to investigate the impact of power grid strength and PLL parameters on stability of grid-connected DFIG wind farm. The flowchart of the proposed approach is depicted in Fig. 3. The detail of how to use this approach will be introduced in the following sections.

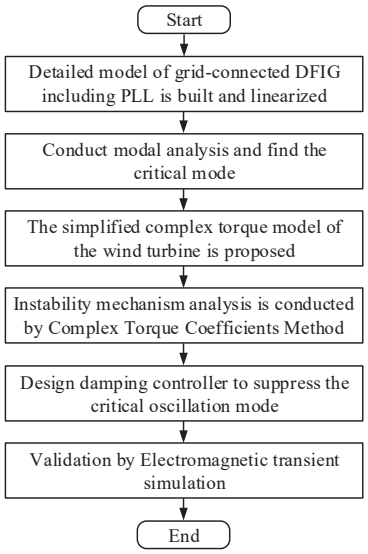

Fig. 3. Flowchart of the proposed approach

III. Eigenvalue Analysis under Different Power Grid Strengths and PLL Parameters

In order to investigate the small signal stability of the grid-connected DFIG wind farm shown in Fig. 2, its dynamic model including the PLL block is established in Matlab/Simulink. And the linearized model is obtained from this non-linear model by using the Control Design Toolbox/Linear Analysis provided in MATLAB [31]. The DFIG depicted in Fig. 2 is an equivalent generator of 5 wind farms. The total rated power of the wind farms is 200 MVA. The base power of the system is 100MVA. The base voltages of all buses are their rated voltages. The parameters of the DFIG could be found in [32]. Then this system is linearized at its equilibrium point, and modal analysis is conducted under different cases. Comparative studies are conducted when the DFIG is operated under the sub-synchronous state, the synchronous state, and the super-synchronous state, respectively. The influences of power grid strengths and PLL parameters are also investigated.

A. Modal Analysis of Grid-Connected DFIG Wind Farm

When the equivalent impedance of the wind power transmission system is Z_{wf}=0.0378+j0.1675, the SCR is S_{tip}=3. The power output of the DFIG is set as 2 p.u.. Modal analysis results are listed in Table I. Since we only concern the conjugate roots, the negative real roots are not listed here. It can be found that there are three oscillation modes in the grid-connected DFIG wind turbine. Mode 1 is related to the equivalent internal d-axis and q-axis voltages $E_d^{'}$, $E_q^{'}$. Thus, it is an oscillation mode associated with stator voltage. The oscillation frequency of this mode is close to 50 Hz and its damping ratio is 1.4%. Mode 2 is mainly related to the two state variables of the PLL block, ω^p and θ^p. The participation factors of all states in the PLL mode are depicted in Fig. 4. Thus it is a PLL oscillation mode. The oscillation frequency of the PLL mode is about 12 Hz and its damping ratio is 48%. Mode 3 is related to the rotor speed ω^r and the torsion angle θ^s of the shaft, thus it is a mechanical oscillation mode. Its oscillation frequency is about 3 Hz and damping ratio is 12%.

TABLE I
MODAL ANALYSIS OF GRID-CONNECTED DFIG

No	Oscillation Frequency	Damping Ratio	Participating Variables	Oscillation Mode
1	49.84	0.014	$E_d^{'}, E_q^{'}$	Stator Voltage
2	12.03	0.475	ω_p, θ_p	PLL
3	3.16	0.117	θ_s, ω_r	Mechanical

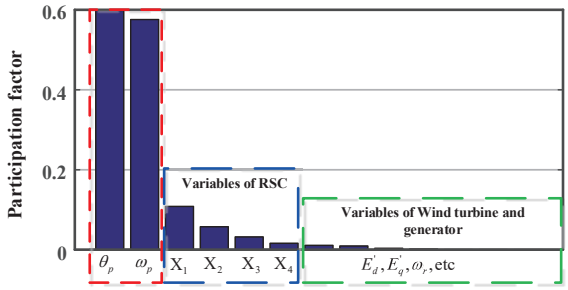

Fig. 4. The participation factor of the states in the PLL mode

B. Oscillatory Characteristics under Sub-synchronous State

When the wind speed is 7.2m/s, the rotor speed of the equivalent DFIG is about 0.8p.u., and the active power output of the DFIG is 0.59 p.u.. By gradually increasing the length of transmission lines, the equivalent impedance Z_{wf} will increase from $0.0218+j0.0932$ to $0.1134+j0.4846$, and then the SCR S_{tip} will decrease from 5.2 to 1 accordingly. The changes of the eigenvalues of the above three concerned modes with S_{tip} are shown in Fig. 5. It can be found that, the mechanical oscillation mode is mainly affected by the state variable θ_s and ω_r. The impact of the power grid strength on those two state variables is relatively small. Thus the damping ratio of the mechanical oscillation mode almost remains constant with the decrease of S_{tip}. Whereas the damping ratio of the stator voltage oscillation mode increases slightly, the damping ratio of the PLL oscillation mode decreases significantly. Since the active power output of the DFIG is relatively small, the load of the transmission line is low. Thus, all the eigenvalues locate in the left half of the complex plane.

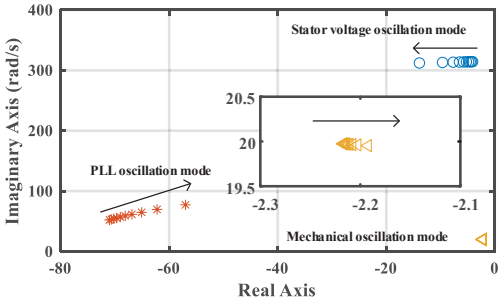

Fig. 5. Dominated eigenvalues of the grid connected DFIG under sub-synchronous state

C. Oscillatory Characteristics under Synchronous State

When the wind speed is regulated, the rotor speed of the equivalent wind turbine changes to 1 p.u. The wind turbine operates at the synchronous state and the active power output is 1.16p.u. With the S_{tip} varies from 5.2 to 1, the eigenvalues of the three concerned modes are shown in Fig. 6. Similar analysis results can be obtained. When S_{tip} decreases, the

eigenvalues of the mechanical oscillation mode almost has no change, whereas the damping ratio of the stator voltage oscillation mode increases slightly, and the damping ratio of the PLL oscillation mode decreases significantly. Although the active power output of the wind farm is still small, the damping ratio of the PLL oscillation mode becomes significantly smaller than that in the sub-synchronous state.

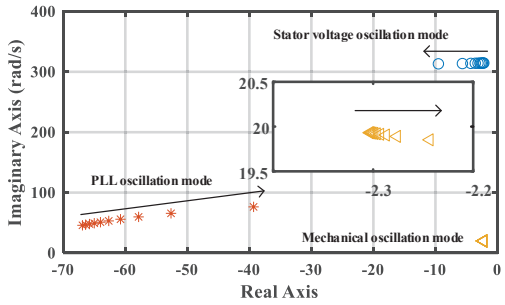

Fig. 6. Dominated eigenvalues of the grid connected DFIG under synchronous state

D. Oscillatory Characteristics under Super-synchronous State

In the rated operation state, the rotor speed of the DFIG is 1.2 p.u. and the active power output is 2 p.u. It is a typical super-synchronous operation state. When the S_{tip} decreases from 5.2 to 1.38 by changing the length of the transmission lines, the eigenvalues of the three concerned modes are shown in Fig.7. It can be found that the damping ratio of the stator voltage oscillation mode increases slightly with the decrease of S_{tip}. However, the damping ratio of the PLL oscillation mode decreases significantly. When S_{tip} equals to 1.38, the load of the transmission line is relatively heavy, and the eigenvalues of the PLL oscillation mode move to the right half of the complex plane. It becomes the first unstable mode. Obviously, when bulk wind power is exported via a long transmission line, the unstable PLL oscillation mode would lead to system instability.

The stability of the DFIG based wind farm is affected by both the power grid strength (the SCR) and the operation state (the power output). It can be observed that the damping ratio of the PLL oscillation mode would decrease when the wind power exported increases or the S_{tip} of the wind power system decreases.

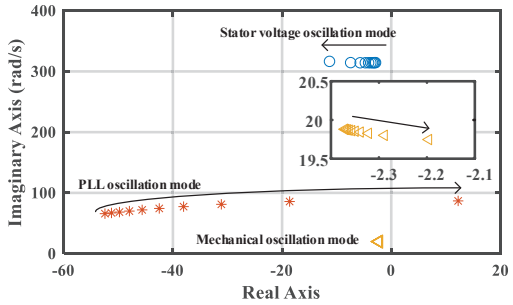

Fig. 7. Dominated eigenvalues of the grid connected DFIG under super-synchronous state

E. Impact of PLL Parameters on Oscillatory Characteristic

As mentioned above, the DFIG connected to a weak grid may easily lose stability under the heavy-duty operating conditions. Thus, the DFIG based wind farm operated under the super-synchronous state is chosen to analyze the impact of PLL parameters on the oscillatory characteristic. Under such a scenario, the SCR at the PCC bus is 1.68 and the integral coefficient K_I of the PLL is 333. When the proportional coefficient K_P of the PLL increases from 20 to 100, the eigenvalues of the oscillation modes are shown in Fig. 8. Since the stator voltage oscillation mode and the mechanical oscillation mode are mainly dominated by the state variables $E_d^{'}$, $E_q^{'}$ and ω_r, θ_s, both the two modes are almost unaffected by the PLL parameters. The eigenvalues of those two oscillation modes slightly change when K_P increases. However, the parameters of the PLL have a significant impact on the PLL oscillation mode. The oscillation frequency of the PLL oscillation mode will increase when K_P increases, and the damping ratio of this oscillation mode will decrease. If the proportional coefficient K_P is too large, the PLL oscillation mode will lose stability.

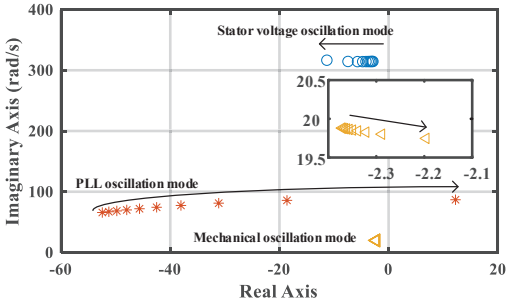

Fig. 8. Dominated eigenvalues of the grid connected DFIG with the increase of the PLL parameters

In summary, both the power grid strength and the operation state can influence the stability of grid-connected wind farm. Especially, the DFIG connected to a weak grid may easily lose stability under the heavy-duty operating conditions. Just like the low frequency oscillation of the conventional synchronous generator, power oscillation of the DFIG based wind farm will occur when bulk wind power delivered via long transmission lines. Thus, if a contingency happens and leads to the outage of one transmission line, the S_{tip} of the power grid would become relatively low. Hence, the system is in the high risk of the oscillation caused by the PLL oscillation mode when the power output of the wind farm is high. Also, the stability of the PLL oscillation mode is affected by the PLL parameters. When the gain of the PLL is too high, the damping ratio of the PLL oscillation mode will become negative, and the oscillation of the wind power system may occur.

IV. Instability Mechanism Analysis by Complex Torque Coefficients Method

To investigate the instability mechanism of the PLL oscillation mode, this section proposes a simplified complex torque model of the wind turbine and investigates the impact of power grid strengths and parameters of PLL on the system stability.

A. Complex Torque Model of the Wind Turbine

Like the complex torque model of the synchronous generator, the structure of PLL can be turned into the format shown in Fig. 7(a). For the convenience of description, it is called

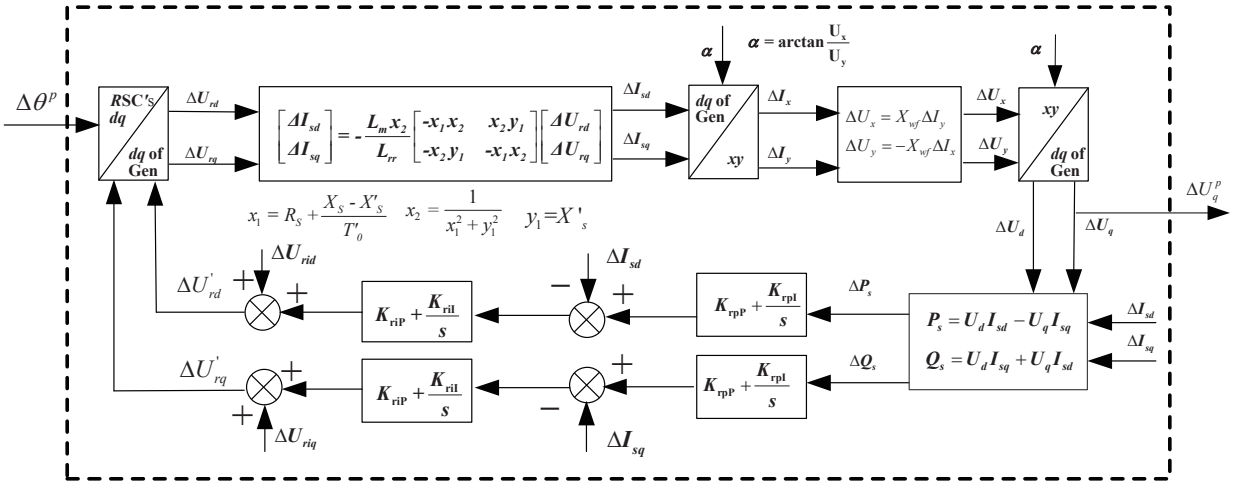

Fig. 10. Diagram of the simplified model $G_1(s)$

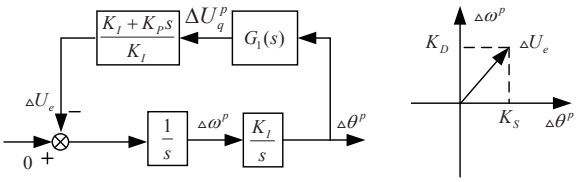

(a) Control loop including PLL block

(b) Vector diagram

Fig. 9. Complex torque analysis of the PLL oscillation mode

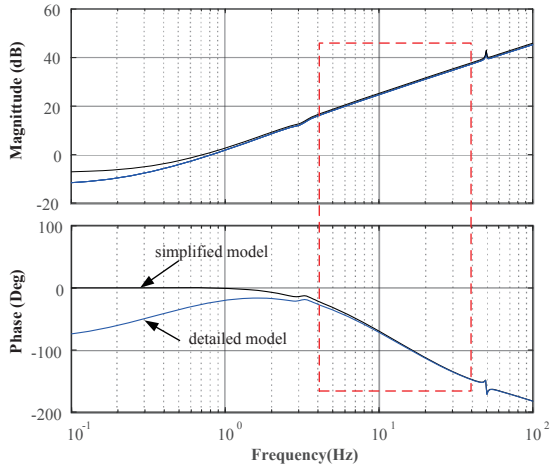

Fig. 11. Bode diagram of the simplified model and detailed model $G_1(s)$

the control loop including the PLL block in this paper. $G_1(s)$ denotes the transfer function from the phase angle $\Delta\theta_p$ to the q-axis bus voltage ΔU_p^q both measured by the PLL.

The transfer function $G_1(s)$ represents other parts of the grid-connected DFIG-WT excluding PLL block. The detailed transfer function of $G_1(s)$ is very complicated and cannot be represented as a simple formula directly. Under a specific operating condition, the bode diagram of $G_1(s)$ can be obtained by linearizing of the nonlinear model of the grid-connected DFIG wind turbine excluding PLL block. According to the participation factor of the states in the PLL mode depicted in Fig. 4, it can be found that the PLL mode is mainly related to the PLL states and controller states of the RSC converter. Therefore, the dynamic states of wind turbine and DFIG can be ignored for analyzing PLL mode only. In addition, the resistor of the long transmission line can also be ignored. Based on the above simplification, a simplified model $G_1(s)$ depicted in Fig. 10 is proposed for analyzing PLL mode. Note that X_{wf} is the equivalent reactance of the wind power transmission system, which is related to SCR of the power grid. $U_{rd}^{'}$ and $U_{rq}^{'}$ are the rotor dq axis voltage in the converter dq-frame. The bode diagram of the simplified model and detailed model $G_1(s)$ is shown in Fig. 11. It can be found that the bode diagram of the simplified model is almost the same as that of the detailed model in the range of 3 to 100Hz. Since the frequency of the PLL mode is around 10Hz, the proposed simplified model can be used for analyzing PLL mode.

According to the complex torque method, the relationship among the voltage deviation ΔU_e measured by the PLL, the phase angle deviation $\Delta\theta^p$, and the frequency deviation is [30]:

$$\Delta U_e = K_S(s)\Delta\theta^p + K_D(s)\Delta\omega^p \tag{9}$$

where, $K_S(s)$ and $K_D(s)$ denote the synchronizing and damping torque coefficient, which are closely related to the oscillation frequency. According to (9), the relationship between the above variables could be illustrated by vectors as shown in Fig. 7(b). If ΔU_e locates in the first quadrant, its projections on the $\Delta\theta^p$ axis and $\Delta\omega^p$ axis are both positive and the system is stable. If ΔU_e locates in the third quadrant, its projection on the $\Delta\omega^p$ axis is negative, the damping of the PLL oscillation mode is negative and the power oscillation may occur. The relationship between the ΔU_e vector and the $\Delta\theta^p$ vector is determined by the following transfer function:

$$G_{PLL}(s) = \frac{\Delta U_e}{\Delta\theta^p} = \frac{K_I + K_P s}{K_I} G_1(s) \tag{10}$$

The location phase of ΔU_e in the complex plane can be obtained by formulating $G_{PLL}(s)$ and calculating its phase angle. Also, the eigenvalues of the PLL oscillation mode can be approximated by [30]:

$$S_{PLL} = -K_D \pm \frac{1}{2}\sqrt{K_D^2 - 4K_I K_S} \tag{11}$$

From (11), it can be concluded that the larger the gain of the control loop including the PLL block is, the larger the $K_S(s)$

and $K_D(s)$ coefficients are, and thus the oscillation frequency of the PLL oscillation mode will also be large.

B. Influence Factors of System Small Signal Stability

According to (10), the phase characteristics of $G_{PLL}(s)$ are determined by $G_1(s)$ and $(K_I + K_P s)/K_I$. The former one is closely related to S_{tip} and the latter one is related to PLL parameters. In the following part, the impact of S_{tip} and PLL parameters on the PLL oscillation mode is investigated.

1) Power Grid Strength: The DFIG is set to operate at the rated state, and the output active power is 2 p.u. With typical PLL parameters ($K_P = 74$, $K_I = 333$), taking $\Delta\theta^p$ as input and ΔU_e as output, the bode diagram of this wind power system under different S_{tip} is shown in Fig. 12. Since the gain of $G_{PLL}(s)$ is more than zero dB, the $G_{PLL}(s)$ control loop would amplify the input signal. Therefore, only when the $G_{PLL}(s)$ is a negative feedback control loop, ΔU_e will be located in the first quadrant, the damping ratio of the PLL mode will be positive. Otherwise, the damping ratio of the PLL mode is negative, and the wind power system could not keep stable.

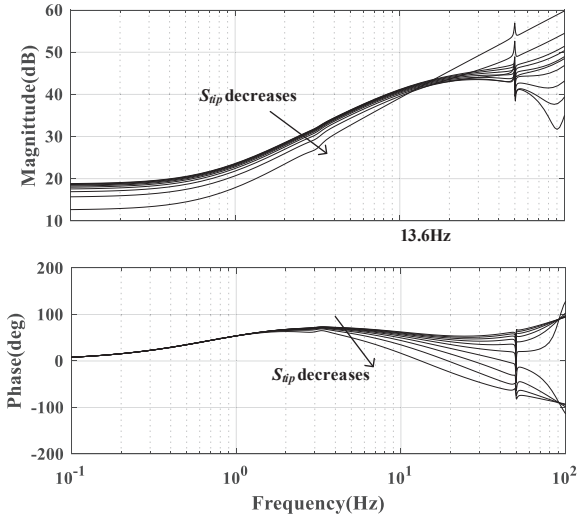

Fig. 12. Bode diagram of open loop PLL control loop under different S_{tip}

From the eigenvalue analysis, it is found that the oscillation frequency of the PLL oscillation mode is 13.6 Hz. Since the gain of the $G_{PLL}(s)$ almost keeps constant around 13.6 Hz when S_{tip} changes, thus the oscillation frequency of the PLL oscillation mode would almost remain unchanged. Assuming that the oscillation frequency of the PLL mode equals to 13.6 Hz, the phase angle $\theta_{G_{PLL}}$ of the $G_{PLL}(s)$ control loop will decrease with the decrease of S_{tip}. Namely, the angle between the ΔU_e vector and $\Delta\theta^p$ vector in the complex plane will decrease accordingly. Thus, the projection of the ΔU_e vector on the $\Delta\omega^p$ axis decreases, and the damping torque coefficient and damping ratio of the PLL mode decrease. Particularly, when S_{tip} decreases to 1.38, $\theta_{G_{PLL}}$ is -6.93 degrees. The vector ΔU_e locates in the fourth quadrant, and its projection on the $\Delta\omega^p$ axis is negative. The PLL oscillation mode will be excited, and the power oscillation of the wind farm will occur. It can be concluded that the damping ratio of the PLL oscillation mode decreases with the decrease of S_{tip}, and the system will be unstable if S_{tip} is lower than a critical value.

2) PLL Parameters: PLL parameters mainly affect the $G_{PLL}(s)$ in two aspects. One is the gain of the control loop including the PLL block. The larger the gain of the control loop including the PLL block is, the higher the oscillation frequency will be. The other is the value of K_P/K_I, which can change the phase-frequency characteristic of the control loop including the PLL block. The larger K_P/K_I is, the larger the phase angle of $(K_I + K_P s)/K_I$ is. In order to investigate the effect of PLL parameters on PLL mode, when S_{tip} is set to be 1.38, the output power of the DFIG is 2 p.u., and K_I is 333, the bode diagrams of $G_{PLL}(s)$ with the K_P increasing from 24 to 84 are shown in Fig. 13.

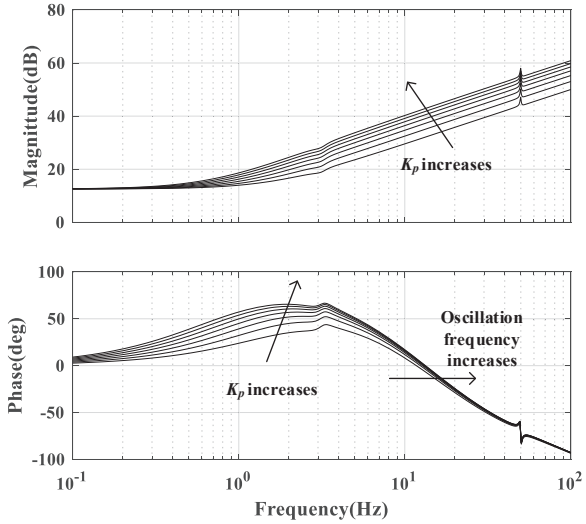

Fig. 13. Bode diagram of the control loop including PLL under different K_P

As shown in Fig. 13, the phase angle of $G_{PLL}(s)$ will increase with the increase of K_P in the low frequency range from 1 to 10 Hz. Thus, the increase of K_P will improve the damping ratio of the oscillation mode in this frequency range. However, the frequency of the PLL mode is about 12 Hz. Even if the value of K_P/K_I changes significantly from 0.07 to 0.25, it has little impact on the phase angle of $(K_I + K_P s)/K_I$ in the high frequency range. As the gain of $(K_I + K_P s)/K_I$ will increase with the increasing of K_P, the magnitude of the vector ΔU_e will increase accordingly, leading to the increase of K_D and K_S. Thus, the oscillation frequency of the PLL mode will also increase. According to Fig. 13, it is easy to find that the phase margin of the PLL mode will decrease with the increase of the oscillation frequency. Thus the damping ratio of the PLL mode will decrease, and the wind power system will lose stability when the oscillation frequency exceeds a critical value. Similarly, if K_I is too large, the gain of the control loop including the PLL block is also high, and the damping ratio of the PLL mode would be negative.

In conclusion, S_{tip} mainly influences the phase frequency characteristics of the control loop including the PLL. The phase margin of the PLL oscillation mode decreases with the decrease of S_{tip}. When S_{tip} is too low, the grid-connected

DFIG wind turbine will lose stability for the PLL mode lacks of damping. PLL parameters mainly influence the oscillation frequency of the PLL mode. If the gain of the control loop including the PLL block increases, the oscillation frequency of the PLL mode will also increase. The wind power system would oscillate for lack of damping. However, if the values of K_P, K_I are too small, the PLL cannot obtain the phase change of the power system accurately. Low gain of the control loop including the PLL block would deteriorate the synchronizing ability of the grid-connected DFIG wind turbine.

V. Damping Controllers Design for DFIG

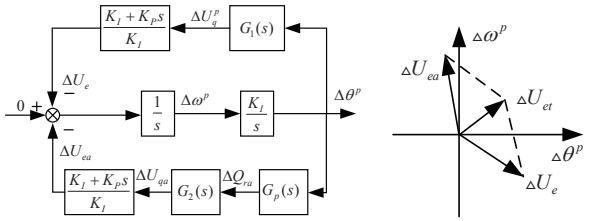

(a) Structure with damping controller (b) Vector diagram

Fig. 14. Complex torque analysis of PLL

To suppress the PLL oscillation, the damping controller shown in Fig. 14 is proposed for the DFIG. This damping controller takes $\Delta\theta^p$ as input and adds its output ΔQ_{ra} on reactive power reference of RSC to form the additional ΔU_{ea} component. $G_2(s)$ is the transfer function from ΔQ_{ra} to the voltage ΔU_{qa}. $G_P(s)$ is the transfer function of the damping controller.

A. Design of Mixed H_2/H_∞ Robust Damping Controller

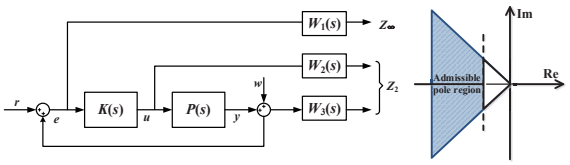

(a) Robust damping controller (b) Pole placement region

Fig. 15. Block diagram of the mixed H_2/H_∞ robust damping controller

In order to achieve the robustness under a wide range of system operating conditions, a mixed H_2/H_∞ robust damping controller (MRDC) is proposed to suppress the PLL oscillation. The configuration of the mixed H_2/H_∞ robust damping controller is shown in Fig. 15(a). To achieve a good response and avoid the fast dynamics and high-frequency gain in the controller, all closed-loop poles are configured in the expected region of the left-half plane, as shown in Fig. 15(b). By applying this multi-objective synthesis approach, the controller could not only has good robustness against uncertainty, but also give good dynamic performance to the system. The detailed description of an LMI approach to such a complex problem of mixed H_2/H_∞ robust damping control with regional pole placement has been given out in [33], [34].

For the single grid-connected DFIG wind farm power system, weighting functions of the controller are given by

$$W_1(s)=\frac{10}{s+10},\quad W_2(s)=0.001,\quad W_3(s)=\frac{40s}{s+40}$$

Thus, the transfer function of the controller $G_P(s)$ for the single-DFIG system depicted in Fig. 2 is,

$$G_P(s)=\frac{0.661s^2+38.33s+89.52}{s^3+6.548s^2+49.6s+19.29}$$

Similarly, the transfer functions of the controller $G_P(s)$ for the multi-DFIG system depicted in Fig. 19 is,

$$G_P(s)=\frac{0.96s^2+19.87s+43.56}{s^3+7.93s^2+22.84s+37.65}$$

B. Design of Phase Compensation Damping Controller

In this paper, the widely used phase compensation damping controller (PCDC) used in [35], [36] is designed for comparison. The PCDC consists of two lead-lag elements and its transfer function is

$$G_P(s)=K_{PC}\frac{T_W s}{1+T_W s}\left(\frac{1+\alpha Ts}{1+Ts}\right)^2 \tag{12}$$

where, T_W is the washout time constant, T and α are the time constant and coefficient of the lead-lag part, respectively, K_{PC} is the gain of the controller.

The parameters of PCDC are designed based on the residue method and the linearization model of the benchmark under a special operation condition. Usually, T_W could be chosen as 3$\sim$10 seconds. In this paper, T_W is chosen to be 3 seconds to isolate the DC component and pass the signal in the PLL oscillation frequency ranges. Thus, the parameters of the PCDC of the single grid-connected DFIG system depicted in Fig. 2 are $\alpha=4, T=0.075, K_{PC}=0.2$, while the parameters of the PCDC designed for the wind turbines in WF A of the multi-DFIG system depicted in Fig. 19 are $\alpha=5.4, T=0.055, K_{PP}=0.6$.

C. Design of LQR-based Damping Controller

In addition, the linear quadratic regulator (LQR) proposed in [37] is also designed for comparison. The detailed design procedure can refer to [37] and is omitted here for page limitation.

Compared with the damping controller proposed in [35]–[37] for DFIG used for damping low frequency oscillations, the proposed mixed H_2/H_∞ damping controller in this paper is used for damping PLL mode. In addition, the conventional lead-lag structure-based damping controller [35], [36] and the LQR-based damping controller [37] are also designed for damping the PLL mode for comparison. Obviously, other advanced control techniques can also be adopted for designing advanced damping controller to improve the damping performance of the PLL mode.

VI. Simulation Validations

A. Single Grid-Connected DFIG System

To validate the effectiveness of the proposed MRDC, the detailed electromagnetic transient model of the grid-connected DFIG wind turbine shown in Fig. 2 is established in P-SCAD/EMTDC environment. The output power of the wind farm is 2 p.u., and is delivered through the double-circuit transmission lines. In this situation, the pre-fault S_{tip} of the wind farm is about 2.5. One of the parallel transmission lines occurs a three-phase-to-ground fault at 3s and is switched off at 3.05s. Consequently, the post-fault S_{tip} of the wind farm decreases to 1.38. The response of the voltage at PCC bus, the frequency deviation at the PCC bus, and the power output of the wind farm are shown in Figs. 16 and 17. It can be found that the post-fault power output of the wind farm oscillates with the frequency about 10Hz. Meanwhile, the frequency deviation of the wind power system measured by the PLL also oscillates with the same frequency. Therefore, it can be concluded that the oscillation of the wind power system is dominated by the PLL mode. It can also be found from Figs. 17 that the MRDC, PCDC, and LQR can suppress the oscillation of the PLL mode effectively. Moreover, the performance of system with the proposed MRDC is better than that of system with the PCDC and is similar to that of system with the LQR. By using the proposed damping controller, the power output of the wind farm could be stabilized, and the frequency deviation measured by the PLL at the PCC bus attenuates to zero rapidly. The resonance phenomenon of the voltage at the PCC bus is also avoided. These simulation results demonstrate that the proposed damping controller could improve the small signal stability of the wind power system at low SCR situation significantly.

To verify the adaptability of the proposed damping controller, the length of wind power transmission lines is increased to set the $S_{tip} = 2.2$ under the nominal operating conditions. When one of the transmission lines is switched off due to the fault at 3 s, the S_{tip} of the wind farm will decrease to 1.2. The responses of the test system at this situation are shown in Fig. 18. Compared with Fig. 17, it can be seen that with the decrease of S_{tip}, the damping ratio of the PLL mode decreases, the frequency deviation oscillates more rapidly and the oscillation magnitude is larger. Similarly, the active power output of wind farm oscillates with larger oscillation magnitude and the beat phenomenon of the voltage at the PCC bus is more evident. Fig. 18 shows that the proposed MRDC is adaptive to different operating conditions. In addition, the performance of the proposed MRDC is slightly better than that of the LQR.

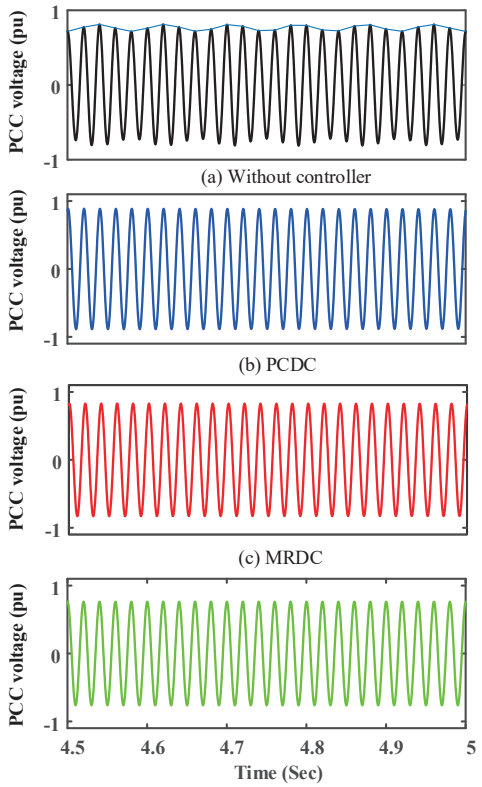

Fig. 16. Response of PCC voltage of the system under the $S_{tip} = 1.38$

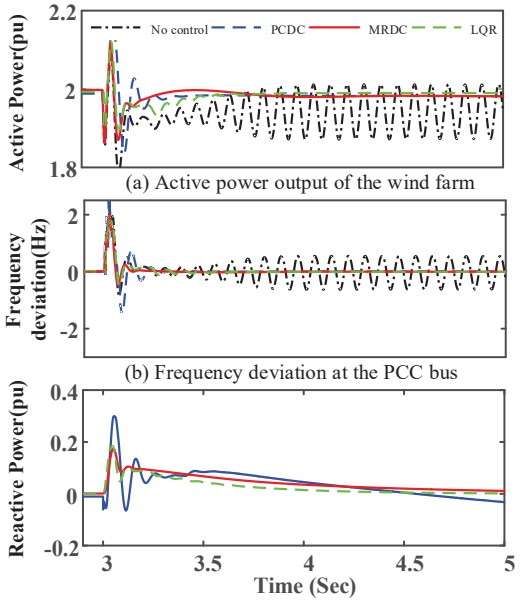

Fig. 17. Response of power output of wind farm and frequency deviation the system under the $S_{tip} = 1.38$

.

B. Multiply Grid-Connected DFIG System

In order to further verify the analysis and validity of the proposed controller, the multiply grid-connected DFIG System depicted in Fig. 19 is used for test system. WF A is composed of five 10MW equivalent wind turbines, whose wind speed is 9, 10, 11.4, 12, 13m/s, respectively. The transmission line 17-18 is replaced with two parallel lines. The detailed parameters of the test system can be found in [38].

At 5s, one of the parallel lines is removed, the response of the system with MRDC, with PCDC, and without damping controller are shown in Fig. 20. When one of the parallel lines is removed, the SCR of the power grid decreases and the damping ratio of the PLL mode is not enough. It can be found from Fig. 20 that the both the MRDC and PCDC can also effectively suppress this PLL oscillation for a multiply

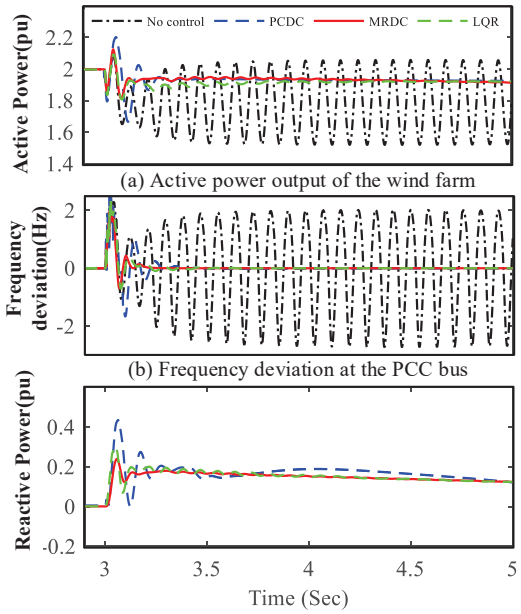

Fig. 18. Response of power output of wind farm and frequency deviation the system under the $S_{tip} = 1.20$

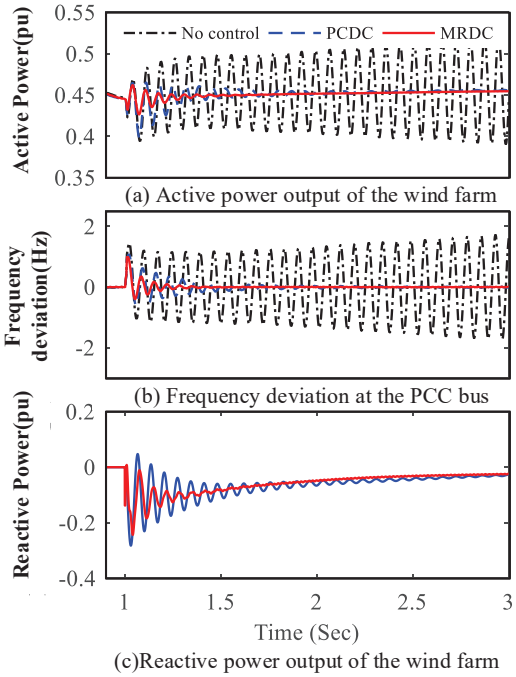

Fig. 20. Response of power output of wind farm and frequency deviation the multi-DFIG system

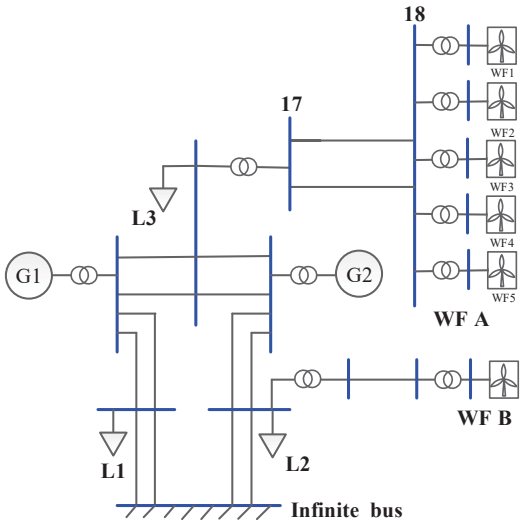

Fig. 19. The multiply grid-connected DFIG system

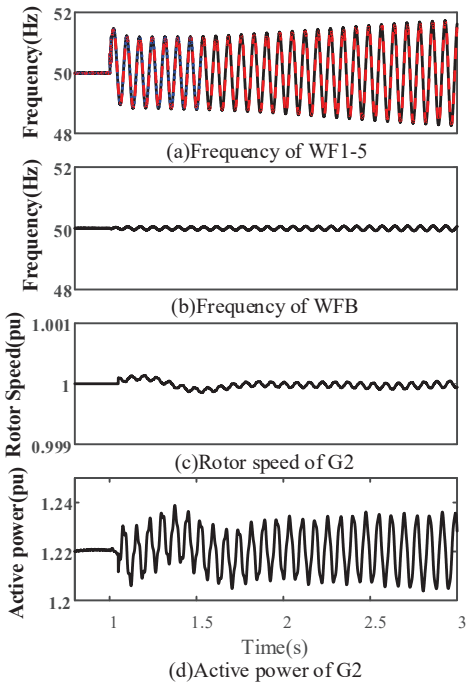

Fig. 21. Response of the multi-DFIG system without the damping controller

grid-connected DFIG System. Moreover, the performance of system with the proposed MRDC is better than that of system with the PCDC. Therefore, both the frequency oscillation of the PCC voltage and the active power oscillations of wind farm will be quickly suppressed. In addition, the frequency response of the each wind turbine in WF A, the frequency response of WF B, rotor speed and active power of G2 under this situation without the damping controller are depicted in Fig. 21. It can be found that both the frequency deviation of WF B and rotor speed deviation of G2 are much less than the frequency deviation of WF A. Therefore, it can be concluded that the PLL mode oscillation is the inner oscillation in WF A and almost no interaction with the synchronous generator and other wind farm.

VII. Conclusions

This paper establishes a dynamic wind turbine model including the detailed characteristics of the PLL block to investigate the power oscillation of the grid-connected DFIG wind turbine. Modal analysis results indicate that the power oscillation phenomenon of the grid-connected DFIG wind turbine is closely related to the oscillation mode dominated by the state variables of PLL block, which is called PLL mode in this paper. Modal analysis results reveal that reason of the DFIG connected to a weak grid may easily lose stability under the

heavy-duty operating conditions. A simplified linear system model of the grid-connected DFIG wind turbine is proposed for analyzing the PLL mode. The frequency response of the closed-loop system including PLL shows that the grid strength at the PCC bus mainly influences the phase characteristics, while the PLL parameters mainly influence the magnitude characteristics. Low grid strength or high gain in the control loops could reduce the damping ratio of the PLL oscillation mode. In order to suppress the power oscillation in PLL mode, a mixed H_2/H_∞ robust damping controller is proposed and designed for grid-connected DFIG. The electromagnetic simulation results of both the single and multiply DFIG systems not only verify the analysis conclusions, but also demonstrates the effectiveness of the proposed mixed H_2/H_∞ robust damping controller. Note that the proposed method can also be generalized to analyze and damp the oscillation phenomenon of the other renewable generation systems like grid-connected photovoltaic system, grid-connected PMSG system. The experimental validation will conducted in our future work.

REFERENCES

[1] L. J. Cai, I. Erlich, "Doubly fed induction generator controller design for the stable operation in weak grids," *IEEE Trans. Sustainable Energy*, vol. 6, no. 3, pp. 1078-1084, May. 2015.

[2] Y. Zhou, D. D. Nguyen, P. C. Kj ær, and S. Saylors,"Connecting wind power plant with weak grid-challenges and solutions," in *Proc. IEEE PES GM*, Vancouver, BC, 2013, pp. 1-7.

[3] J. Liu, J. Y. Wen, W. Yao, and Y. Long, "Solution to short-term frequency response of wind farms by using energy storage systems," *IET Renewable Power Gener.*, vol. 10, no. 5, pp. 669-678, Apr. 2016.

[4] S. S. Baghsorkhi and I. A. Hiskens, "Analysis tools for assessing the impact of wind power on weak grids," in *Proc. IEEE International Systems Conference*, Vancouver, BC, 2012, pp. 1-8.

[5] O. Noureldeen and I. Hamdan, "Design of robust intelligent protection technique for large-scale grid-connected wind farm," *Protection and Control of Modern Power Systems*, vol. 3, no. 3, pp.169-182, Jun. 2018.

[6] B. Yang, T. Yu, H. C. Shu, J. Dong, and L. Jiang, "Robust sliding-mode control of wind energy conversion systems for optimal power extraction via nonlinear perturbation observers," *Appl. Energy*. vol. 210, pp. 711-723, Jan. 2018.

[7] J. Chen , W. Yao ,C. K. Zhang, Y. Ren, and L. Jiang, "Design of robust MPPT controller for grid-connected PMSG-Based wind turbine via perturbation observation based nonlinear adaptive control," *Renewable Energy*, vol, 134, pp. 478-495, Apr. 2019.

[8] S. W. Liao, W. Yao, X. N. Han, J. Y. Wen, and S. J. Cheng, "Chronological operation simulation framework for regional power system under high penetration of renewable energy using meteorological data," *Appl. Energy*, vol. 203, pp. 816-828, Oct. 2017.

[9] K. Narendra, D. Fedirchuk, R. Midence, N. Zhang, A. Mulawarman, P. Mysore, and V. Sood, "New microprocessor based relay to monitor and protect power systems against sub-harmonics," in *Proc. IEEE Electrical Power and Energy Conference*, Winnipeg, MB, 2011, pp. 438-443.

[10] I. Hr, R. J. Best, and D. J. Morrow, "Inter-area power oscillation frequency mode with wind turbine generator in Irish power system using PMU data," in *Proc. 48th Int. UPEC*, Dublin, 2013, pp. 1-5.

[11] R. K. Varma and A. Moharana, "SSR in double-cage induction generator-based wind farm connected to series-compensated transmission line," *IEEE Trans. Power Syst.*, vol. 28, no. 3, pp. 2573-2583, Aug. 2013.

[12] H. A. Mohammadpour, A. Ghaderi, and E. Santi, "Analysis of subsynchronous resonance in doubly-fed induction generator-based wind farms interfaced with gate-controlled series capacitor," *IET Gener. Transm. Distrib.*, vol. 8, no. 12, pp. 1998-2011, Dec. 2014.

[13] A. E. Leon and J. A. Solsona, "Sub-synchronous interaction damping control for DFIG wind turbines," *IEEE Trans. Power Syst.*, vol. 30, no. 1, pp. 419-428, Jan. 2015.

[14] W. Chen, X. Xie, D. Wang, H. K. Liu, and H. Liu, "Probabilistic stability analysis of subsynchronous resonance for series-compensated DFIG-based wind farms," *IEEE Trans. Sustainable Energy*, vol. 9, no. 1, pp. 400-409, Jan. 2018.

[15] D. S. Yang, X. F. Wang, F. C. Liu, K. Xin, Y. F. Liu, and F. Blaabjerg, "Adaptive reactive power control of PV power plants for improved power transfer capability under ultra-weak grid conditions," *IEEE Trans. Smart Grid*, 2018, in press.

[16] L. Zhang, L. Harnefors, and H. Nee, "Interconnection of two very weak AC systems by VSC-HVDC links using power-synchronization control," *IEEE Trans. Power Syst.*, vol. 26, no. 1, pp. 344-355, Feb. 2011.

[17] J. Z. Zhou, H. Ding, S. Fan, Y. Zhang, and A. M. Gole, "Impact of short-circuit ratio and phase-locked-loop parameters on the small-signal behavior of a VSC-HVDC converter," *IEEE Trans. Power Del.*, vol. 29, no. 5, pp. 2287-2296, Oct. 2014.

[18] M. F. M. Arani and Y. A. R. I. Mohamed, "Analysis and performance enhancement of vector-controlled VSC in HVDC links connected to very weak grids," *IEEE Trans. Power Syst.*, vol. 32, no. 1, pp. 684-693, Jan. 2017.

[19] A. Egea-Alvarez, S. Fekriasl, F. Hassan, and O. Gomis-Bellmunt, "Advanced vector control for voltage source converters connected to weak grids," *IEEE Trans. Power Syst.*, vol. 30, no. 6, pp. 3072-3081, Nov. 2015.

[20] L. L. Fan and Z. X. Miao, "Wind in weak grids: 4 Hz or 30 Hz Oscillations?," *IEEE Trans. Power Syst.*, vol. 33, no. 5, pp. 5803-5804, Sep. 2018.

[21] L. L. Fan, "Modeling type-4 wind in weak grids" *IEEE Trans. Sustainable Energy*, 2018, in press.

[22] L. L. Fan and Z. X. Miao, "An explanation of oscillations due to wind power plants weak grid interconnection," *IEEE Trans. Sustainable Energy*, vol. 9, no. 1, pp. 488-490, Jan. 2018.

[23] D. Zhang, Y. Wang, J. Hu, S. Ma, Q. He, and Q. Guo, "Impacts of PLL on the DFIG-based WTG's electromechanical response under transient conditions: analysis and modeling," *CSEE J. Power Energy Syst.*, vol. 2, no. 2, pp. 30-39, Jun. 2016.

[24] X. Xi, H. Geng, and G. Yang, "Enhanced model of the doubly fed induction generator-based wind farm for small-signal stability studies of weak power system," *IET Renewable Power Gener.*, vol. 8, no. 7, pp. 765-774, Sep. 2014.

[25] Ö. G ö ksu, R. Teodorescu, C. L. Bak, F. Iov, and P. C. Kjær, "Instability of wind turbine converters during current injection to low voltage grid faults and PLL frequency based stability solution," *IEEE Trans. Power Syst.*, vol. 29, no. 4, pp. 1683-1691, Jul. 2014.

[26] J. Hu, Q. Hu, B. Wang, H. Tang, and Y. Chi, "Small signal instability of PLL-synchronized Type-4 wind turbines connected to high-impedance ac grid during LVRT," *IEEE Trans. Energy Convers.*, vol. 31, no. 4, pp. 1676-1687, Dec. 2016.

[27] J. Hu, Y. Huang, D. Wang, H. Yuan, and X. Yuan, "Modeling of grid-connected DFIG-based wind turbines for DC-link voltage stability analysis," *IEEE Trans. Sustainable Energy*, vol. 6, no. 4, pp. 1325-1336, Oct. 2015.

[28] Z. Wang, C. Shen, and F. Liu, "Impact of DFIG with phase lock loop dynamics on power systems small signal stability," in *Proc. IEEE PES GM Conf. & Expo.*, National Harbor, MD, 2014, pp. 1-5.

[29] Y. W. Zheng and Y. D. Li, "Stability analysis of doubly-fed wind power generation system based on phase-locked loop," in *Proc. ICMES*, Wuhan, 2008, pp. 2251-2254.

[30] K. Givaki and L. Xu, "Stability analysis of large wind farms connected to weak AC networks incorporating PLL dynamics," in *Proc. Int. Conf. on RPG*, Beijing, 2015, pp. 1-6.

[31] MATALB document, "Control System Toolbox User's Guide R2016a," *The Math Works Inc*, 2016.

[32] F. Mei and B. C. Pal, "Modal analysis of grid-connected doubly fed induction generators," *IEEE Trans. Energy Convers.*, vol. 22, no. 3, pp. 728-736, Sep. 2007.

[33] C. Scherer, P. Gahinet, and M. Chilali, "Multiobjective output-feedback control via LMI optimization," *IEEE Trans. Autom. Control*, vol.42, no. 7, pp. 896-911, Jul. 1997.

[34] Y. Li, C. Rehtanz, S. Ruberg, L. F. Luo, and Y. J. Cao, "Wide-area robust coordination approach of HVDC and FACTS Controllers for damping multiple interarea oscillations," *IEEE Trans. Power Delivery*, vol. 27, no. 3, pp. 1096-1105, Jul. 2012.

[35] F. M. Hughes, O. Anaya-Lara, N. Jenkins, and G. Strbac, "A power system stabilizer for DFIG-based wind generation," *IEEE Trans. Power Syst.*, vol. 21, no. 2, pp. 763-772, May 2006.

[36] H. Geng, X. Xi, L. Liu, G. Yang, and J. Ma, "Hybrid modulated active damping control for DFIG-based wind farm participating in frequency response," *IEEE Trans. Energy Convers.* , vol. 32, no, 3, pp. 1220-1230, Sep. 2017.
[37] G. P. Prajapat, N. Senroy, and I. Narayan Kar, "Stability enhancement of DFIG-based wind turbine system through linear quadratic regulator," *IET Gener. Transm. Distrib.*, vol. 12, no. 6, pp. 1331-1338, Mar. 2018.
[38] S. M. Muyeen, R. Takahashi, M. H. Ali, T. Murata, and J. Tamura, "Transient stability augmentation of power system including wind farms by using ECS," *IEEE Trans. Power Syst.*, vol. 23, no. 3, pp. 1179-1187, Aug. 2008.

Ju Liu received the B.Eng. and Ph.D. degrees in electrical engineering from the Huazhong University of Science and Technology (HUST), Wuhan, China, in 2011 and 2016, respectively.

He is currently working at the State Grid Hubei economic and research institute. His current research interests include renewable energy, power system analysis, and power grid planning.

Wei Yao (M'13-SM'17) received the B.S. and Ph.D. degrees in electrical engineering from Huazhong University of Science and Technology (HUST), Wuhan, China, in 2004 and 2010, respectively.

He was a Post-Doctoral Researcher with the Department of Power Engineering, HUST, from 2010 to 2012 and a Postdoctoral Research Associate with the Department of Electrical Engineering and Electronics, University of Liverpool, Liverpool, U.K., from 2012 to 2014. Currently, he has been an Associate Professor with the School of Electrical and Electronics Engineering, HUST, Wuhan, China. His current research interests include power system stability analysis and control, HVDC & FACTS, and renewable energy.

Jinyu Wen (M'10) received the B.S. and Ph.D. degrees in electrical engineering from Huazhong University of Science and Technology (HUST), Wuhan, China, in 1992 and 1998, respectively.

He was a Visiting Student from 1996 to 1997 and Research Fellow from 2002 to 2003 all at the University of Liverpool, Liverpool, UK, and a Senior Visiting Researcher at the University of Texas at Arlington, Arlington, USA, in 2010. From 1998 to 2002 he was a Director Engineer with XJ Electric Co. Ltd. in China. In 2003, he joined the HUST and now is a Professor with the School of Electrical and Electronics Engineering, HUST. His current research interests include renewable energy integration, energy storage, multi-terminal HVDC and power system operation and control.

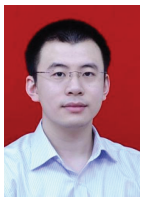

Jiakun Fang (S'10-M'13) received the B.Sc. and Ph.D. degrees from Huazhong University of Science and Technology (HUST), China, in 2007 and 2012, respectively.

He was with Huazhong University of Science and Technology (HUST), Wuhan, China. Currently he is an Associate Professor with the Department of Energy Technology, Aalborg University, Aalborg, Denmark. His research interests include power system dynamic stability control, power grid complexity analysis and integrated energy system.

L. Jiang (M'00) received the B.Sc. and M.Sc. degrees from Huazhong University of Science and Technology (HUST), Wuhan, China in 1992 and 1996, respectively, and the Ph.D. degree from the University of Liverpool, Liverpool, U.K., in 2001, all in electrical engineering.

He was a Postdoctoral Research Assistant with The University of Liverpool, Liverpool, U.K., from 2001 to 2003 and a Postdoctoral Research Associate with the Department of Automatic Control and Systems Engineering, University of Sheffield, Sheffield, U.K., from 2003 to 2005. He was a Senior Lecturer with the University of Glamorgan from 2005 to 2007 and joined the University of Liverpool in 2007. Currently, he is a Reader with the Department of Electrical Engineering and Electronics, The University of Liverpool. His current research interests include control and analysis of power system, smart grid, and renewable energy.

Haibo He (F'17) received the B.S. and M.S. degrees in electrical engineering from Huazhong University of Science and Technology, China, in 1999 and 2002, respectively, and the Ph.D. degree in electrical engineering from Ohio University in 2006. From 2006 to 2009, he was an Assistant Professor at the Department of Electrical and Computer Engineering at Stevens Institute of Technology. Currently, he is the Robert Haas Endowed Chair Professor at the Department of Electrical, Computer, and Biomedical Engineering at the University of Rhode Island. His research interests include adaptive dynamic programming, computational intelligence, machine learning and data mining, and various applications. He has published 1 sole-author research book (Wiley), edited 1 book (Wiley-IEEE) and 6 conference proceedings (Springer), and authored and co-authored over 250 peer-reviewed journal and conference papers. He severed as the General Chair of the IEEE Symposium Series on Computational Intelligence (SSCI 2014). He was a recipient of the IEEE International Conference on Communications Best Paper Award (2014), IEEE Computational Intelligence Society (CIS) Outstanding Early Career Award (2014), National Science Foundation (NSF) CAREER Award (2011), and Providence Business News (PBN) Rising Star Innovator Award (2011). Currently, he is the Editor-in-Chief of the IEEE Transactions on Neural Networks and Learning Systems.

Shijie Cheng (M'86-SM'87-F'11-LF'18) received the B.S. degree from Xi'an Jiaotong University, Xi'an, China, in 1967, the M.Sc. degree from Huazhong University of Science and Technology (HUST), Wuhan, China, in 1981, and the Ph.D. degree from the University of Calgary, Calgary, AB, Canada, in 1986, all in the electrical engineering.

He has been a Professor with the School of Electrical and Electronics Engineering, HUST, Wuhan, China, since 1991. His research interests are power system control, stability analysis, application of Artificial Intelligence, and energy storage.

Prof. Cheng is a Fellow of the Chinese Academy of Sciences.